Icarus 000 (2017) 1–13

Contents lists available at ScienceDirect

Icarus

journal homepage: www.elsevier.com/locate/icarus

Pluto: Pits and mantles on uplands north and east of Sputnik Planitia

Alan D. Howard[a,*], Jeffrey M. Moore[b], Oliver L. White[b], Orkan M. Umurhan[b], Paul M. Schenk[c], William M. Grundy[d], Bernard Schmitt[e], Sylvain Philippe[e], William B. McKinnon[f], John R. Spencer[g], Ross A. Beyer[h,b], S. Alan Stern[g], Kimberly Ennico[g], Cathy B. Olkin[g], Harold A. Weaver[i], Leslie A. Young[b], the New Horizons Science Team

[a] Department of Environmental Sciences, University of Virginia, Charlottesville, VA 22904, USA
[b] National Aeronautics and Space Administration (NASA) Ames Research Center, Space Science Division, Moffett Field, CA 94035, USA
[c] Lunar and Planetary Institute, Houston, TX 77058, USA
[d] Lowell Observatory, Flagstaff, AZ, USA
[e] Université Grenoble Alpes, CNRS, IPAG, F-38000 Grenoble, France
[f] Department of Earth and Planetary Sciences, Washington University, St. Louis, MO 63130, USA
[g] Southwest Research Institute, Boulder, CO 80302, USA
[h] The SETI Institute, Mountain View, CA 94043, USA
[i] The Johns Hopkins University, Applied Physics Laboratory, Laurel, MD 20723, USA

A R T I C L E I N F O

Article history:
Received 6 December 2016
Revised 18 February 2017
Accepted 28 February 2017
Available online xxx

Keywords:
Pluto, surface
Ices
Geological processes

A B S T R A C T

The highlands region north and east of Sputnik Planitia can be subdivided into seven terrain types based on their physiographic expression. The northern rough uplands are characterized by jagged uplands and broad troughs, and it may contain a deeply-eroded ancient mantle. Dissected terrain has been interpreted to have been eroded by paleo-glaciation. The smooth uplands and pits terrain contains broad, rolling uplands surrounding complexes of pits, some of which contain smooth floors. The uplands are mantled by smooth-surfaced deposits possibly derived from adjacent pits through low-power explosive cryovolcanism or through slow vapor condensation. The eroded smooth uplands appear to have originally been smooth uplands and pits terrain modified by small-scale sublimation pitting. The bright pitted uplands features intricate texturing by reticulate ridges that may have originated by sublimation erosion, volatile condensation, or both. The bladed terrain is characterized by parallel ridges oriented north–south and is discussed in a separate paper. The dark uplands are mantled with reddish deposits that may be atmospherically deposited tholins. Their presence has affected long-term landform evolution. Widespread pit complexes occur on most of the terrain units. Most appear to be associated with tectonic lineations. Some pits are floored by broad expanses of ices, whereas most feature deep, conical depressions. A few pit complexes are enclosed by elevated rims of uncertain origin.

1. Introduction

A ring of uplands extends 3.5–4.5 km above the N_2-rich ice-mantled Sputnik Planitia[1] (formerly called Sputnik Planum by the New Horizons mission team) on its northern and eastern edges (Fig. 1).

These uplands have been interpreted to be an ancient, strongly modified rim complex of a ~1200 km impact basin that contains Sputnik Planitia [***SP***] (Schenk et al., 2015; Johnson et al., 2016), although a competing explanation suggests depression of the ***SP*** resulting from a runaway accumulation of N_2 (Hamilton et al., 2016). These uplands feature a diverse landscape of constructional and erosional features, including large degraded craters, modern glaciers, valleys interpreted to have formed through paleo-glaciation (Howard et al., 2017; Moore et al., 2016), steep linear ridges called bladed terrain, and the pitted and mantled terrains emphasized here. This is one of several papers detailing the surface geomorphology and landforms of Pluto's encounter hemisphere (Moore et al., 2017; Howard et al., 2017; White et al., 2017).

* Corresponding author.
E-mail address: ah6p@virginia.edu (A.D. Howard).

[1] All place names on Pluto are informal.

http://dx.doi.org/10.1016/j.icarus.2017.02.027
0019-1035/© 2017 Elsevier Inc. All rights reserved.

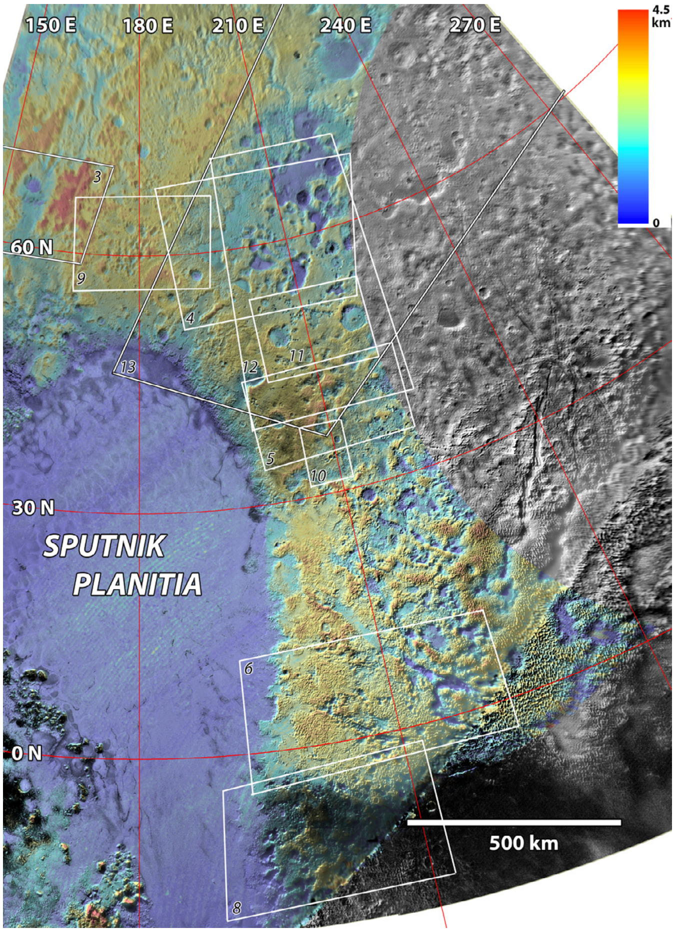

Fig. 1. Landforms north and east of the informally named Sputnik Planitia. Locations of other figures shown by numbered boxes. Lambert conformal conic projection with standard parallels of 0°N and 50°N, with central meridian 180°E. Unless noted otherwise, images in all figures are PEMV_01_P_MVIC_LORRI_CA (340 m/pixel) in regions with color elevation overlay and PEMV_01_P_Mpan1 (495 m/pixel) in other areas except for lower-resolution coverage at southern latitudes. Stereo anaglyph images are based on these two image sets.

2. Landforms of highlands north and east of Sputnik Planitia

In this section we identify seven broad landscape terrains on the northern and eastern margins of ***SP*** as well as four smaller landform types that are distributed across all of the terrains.

2.1. Landscape terrains

Proceeding clockwise from north the terrains are (Fig. 2a):

2.1.1. Northern rough uplands

The region extending northwards from ***SP*** to and beyond the North Pole features a rough-hewn series of ridges, plateaus, and broad depressions with local relief exceeding 1.5 km (Figs. 2a, 3, and S1). Parallel troughs 10–20 km wide, oriented north–south, and 100–200 km long dissect the uplands and may result from a hemispheric fracture system that extends southward along the western margin of ***SP***.

2.1.2. Dissected terrain

This terrain features a variety of linear depressions (valleys) with locally distinct morphologies, including fluted, dendritic, and mountainous expressions (Fig. 2a, linear depressions on uplands in left side of Fig. 4). These valleys are interpreted to have been eroded by paleo-glacial nitrogen ice flows (Howard et al., 2017) which were more extensive than the modern N_2 glaciers along the eastern margin of ***SP***. A glacial origin was concluded because the thin atmosphere of Pluto and the low yearly solar flux makes a nitrogen hydrological cycle involving appreciable liquid runoff unlikely, although it has been suggested that short duration warming epochs during the ~3 Ma obliquity cycle might raise surface temperatures to the melting point of N_2 (Stern et al., 2016). A paleo-inventory of a kilometer or more of nitrogen ice on the uplands surrounding SP would be sufficient to cause basal melting under reasonable geotherms. In addition, the valley systems display irregular profiles, which can occur under confined sub-glacial drainage.

2.1.3. Smooth uplands and pits

This region features relatively smooth-textured uplands that rise abruptly a kilometer or more above adjacent large pits and flat-floored depressions (Figs. 2a, 4 and S2). The smoothness of these uplands (e.g., at ‘a’–‘d’ in Fig. 4) suggests that they are covered by thick mantles. The boundary between smooth uplands and eroded smooth uplands follows the discontinuous, northwest-facing ridge system informally named Eriksson Rupes along its eastern edge (e.g. the ridges southeast of ‘a’ and ‘b’ in Fig. 4).

2.1.4. Eroded smooth uplands

This terrain resembles in broad topographic pattern the smooth uplands and pits, with broadly contoured uplands over distances of tens of km interrupted by pits, lowlands, and ancient crater basins (Figs. 2a and 5). It is distinguished from the smooth uplands and pits terrain by a rough texture at decameter to km scale. The boundary between smooth uplands and pits and eroded smooth uplands is indistinct and may be transitional.

2.1.5. Bright pitted uplands

This high-albedo upland to the east of ***SP*** (eastern Tombaugh Regio) features modern glaciers along its western border that drain into ***SP*** (Figs. 2a, 6, 7 and S3) (Howard et al., 2017; Moore et al., 2016). East of the glaciers the landscape features smooth, irregularly shaped shallow basins typically a few tens of km in width interspersed with a quasi-cellular (reticulate) pattern of ridges. The ridges are typically spaced 5–10 km apart forming a pitted terrain. The reticulate landforms have presumably formed by an uncertain combination of sublimation forming the pits and perhaps cold-trap deposition forming the rims (Moore et al., 1999, 2016; Howard and Moore, 2008).

2.1.6. Bladed terrain

A high plateau is sculpted into largely N–S oriented narrow ridges spaced about 5–10 km apart (Figs. 1, 2a, 6, and S5). These ridges, or blades, are distinguished from the reticulate ridges on the bright pitted uplands by the consistent orientation of the former and their distinctive bluish-gray coloration in visible light. The properties and possible origin of this terrain is the subject of a companion paper (Moore et al., in preparation).

2.1.7. Dark uplands

A low-albedo terrain (Krun Macula) borders the bright pitted uplands to the south along a sharp albedo contrast (Figs. 1, 2a, and 8). Similar low-albedo terrain (Cthulhu Regio) borders the western margin of SP at the same equatorial latitude. The mantle of tholins in Cthulhu Regio is thought to be relatively thin compared to the topographic relief (Grundy et al., 2016). It is likely to be thin in the dark uplands terrain as well, but the landforms in this region differ strongly from the bright pitted uplands. Both the cellular ridges and icy flats of the latter are absent; rather the topography in the dark uplands terrain consists of a rough upland plateau interrupted by troughs and basins up to 3 km deep and 20 km wide.

Please cite this article as: A.D. Howard et al., Pluto: Pits and mantles on uplands north and east of Sputnik Planitia, Icarus (2017), http://dx.doi.org/10.1016/j.icarus.2017.02.027

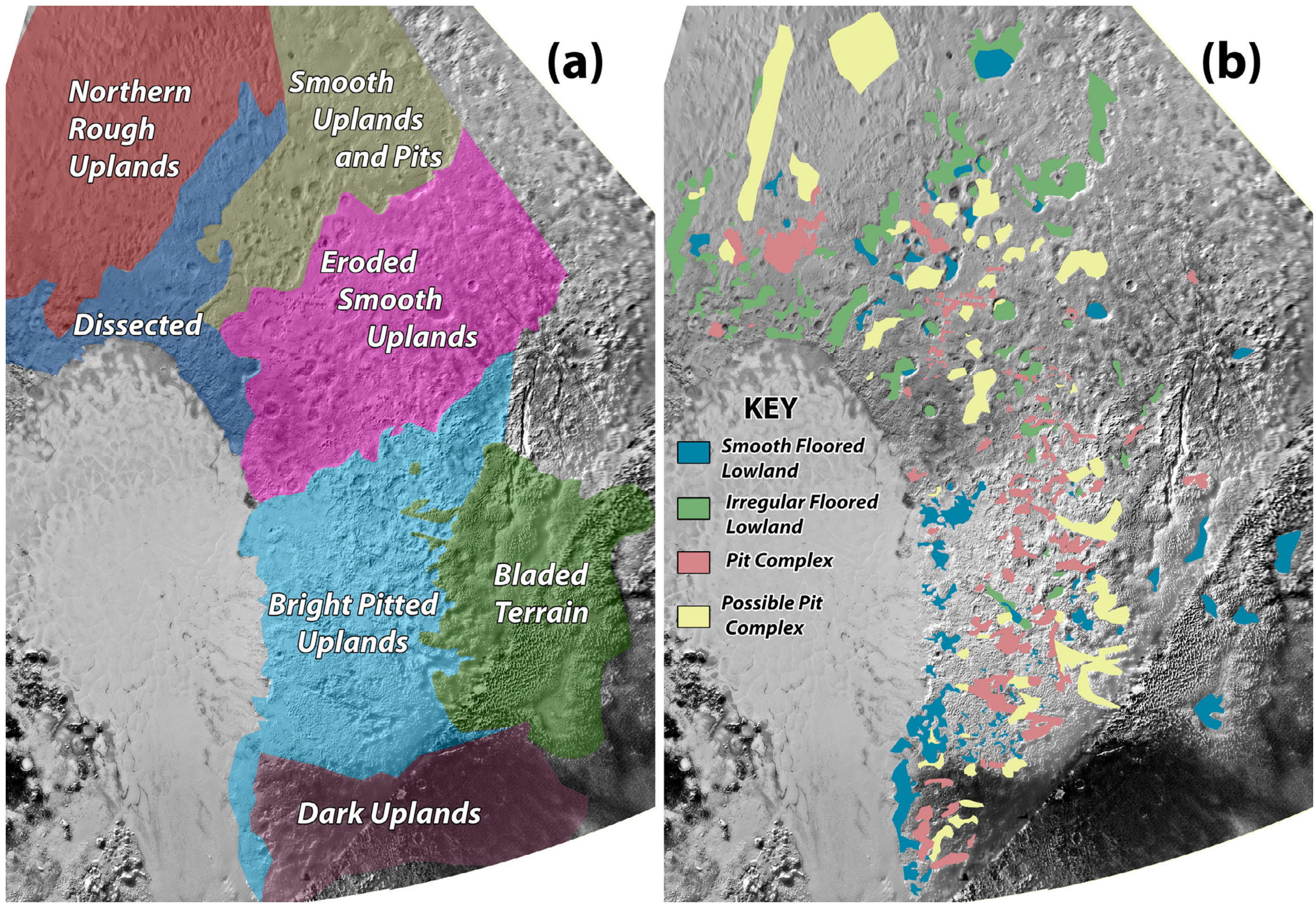

Fig. 2. Mapped regions and features. (a) Terrain map; (b) Feature map. See Fig. 1 for scale and latitude–longitude overlay. Lambert conformal conic projection with standard parallels of 0°N and 50°N, with central meridian 180°E.

2.2. Topographic units

These distinctive broad regions, however, share a suite of landforms at the tens-of-kilometers scale, including pit complexes and lowland plains. Interpretation of the origin of these topographic units in the context of the terrains hosting them constitutes the major topic of this paper. In Fig. 2b we map the distribution of four distinctive units:

2.2.1. Pit complexes

At numerous locations within the study area sharp-edged, relatively circular pits 5–20 km in diameter occur as clusters (Figs. 2b, 7, 9, 10, 11, and S4–S6). In some locations the pits adjoin each other, forming dense complexes as much as 75–100 km across. In other locations they are organized into linear chains. Individual small pits cannot be distinguished from impact craters, but were grouped together their attribution as pit complexes become clear. Some of the larger, steep-walled pits extend more than 4 km below surrounding terrain. Some pits have smooth floors up to tens of km wide—the floors of such pits are mapped as smooth-floored lowlands (Figs. 2b, 4, 12, and S2). Sharp marginal scarps surround many of the conical and flat-floored pits units in both the smooth mantled and bright pitted uplands regions (e.g. Figs. 3, 6, 8, 9, and S2–S7). These scarps are 1–2.6 km in relative relief with gradients ranging from ~20%–45%, although the gradients may be underestimated because of limitations of photogrammetric topographic mapping. Many pits, however, have a smooth conical shape suggesting they may be at the angle of repose (~30°–45°). Pit complexes are easy to distinguish in otherwise relatively low-relief terrain, such as the dissected and smooth uplands terrains. In high-relief terrain like the bright pitted uplands, pit complexes can be distinguished from reticulate landforms only where the pits are large and tightly clustered or are aligned along obvious structural lineations. The class of features most difficult to distinguish from pit complexes is the cellular ridge and pits of the bright pitted uplands, which contains both morphologies (e.g. Figs. 6 and 7). The ridges of the bright pitted uplands, however, extend above the surrounding terrain and have a reasonably uniform scale and spatial organization. What we map as pit complexes in this region are large, and are generally located on well-defined structural trends.

In most locations individual pits and pit complexes are separated from adjoining uplands by sharp breaks in slope, and, where pits adjoin, by sharp divides (Figs. 4, 9, and S2–S5). Some pit complexes, however, are distinguished by elevated rims. Sharp-crested rims in eroded smooth uplands terrain are illustrated in Fig. 10, and possibly by some pits on the right side of Fig. S3 in the bright pitted uplands. Both conical and flat-floored pits in the smooth uplands terrain, however, have broad, rounded elevated rims (Figs. 4, 12, and S2). The highest ridges of the smooth uplands terrain lie within 5–10 km of adjacent pits and depressions, and, where the depressions are widely spaced, the upland gradually decrease in elevation away from the crest over a distance of 15–30 km, forming a strongly asymmetrical topographic profile. Where depressions are closely spaced, the ridge profiles are more symmetrical; these ridges are, however, higher than uplands more distant from

Please cite this article as: A.D. Howard et al., Pluto: Pits and mantles on uplands north and east of Sputnik Planitia, Icarus (2017), http://dx.doi.org/10.1016/j.icarus.2017.02.027

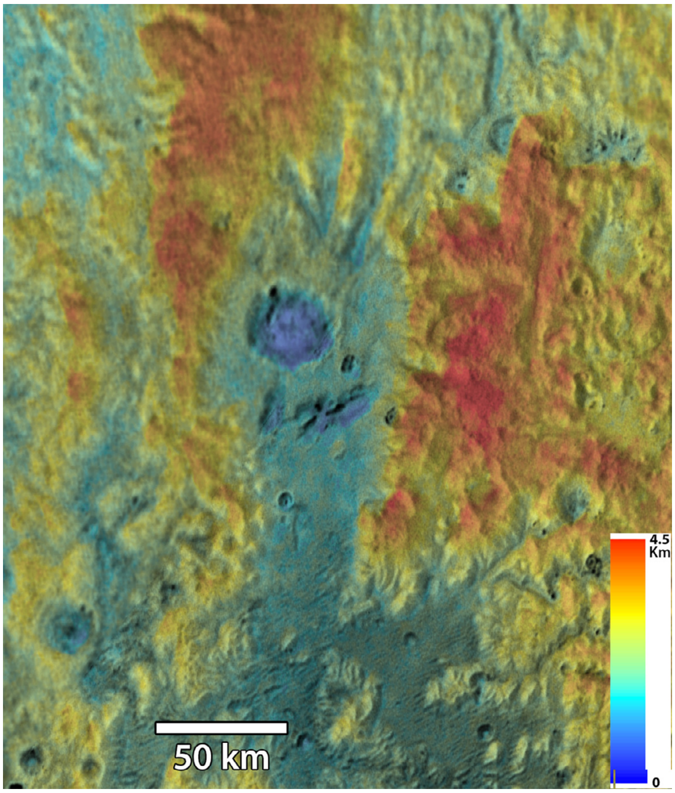

Fig. 3. Northern rough uplands. Lambert conformal conic projection with standard parallels of 30°N and 50°N, with central meridian 150°E. North to top. Image centered at about 156.5°E, 67.8°N. Note irregular, dissected topography with dominant north–south depressions and ridges along presumed tectonic lineations. Elevation scale in km. Several 10+ km diameter craters are visible. See Fig. S1 for anaglyph image of region. See Fig. 1 for location. PELR_P_LORRI mosaic at 890 m/pixel. Unless otherwise indicated on the figures in this paper, north is toward the top of the image.

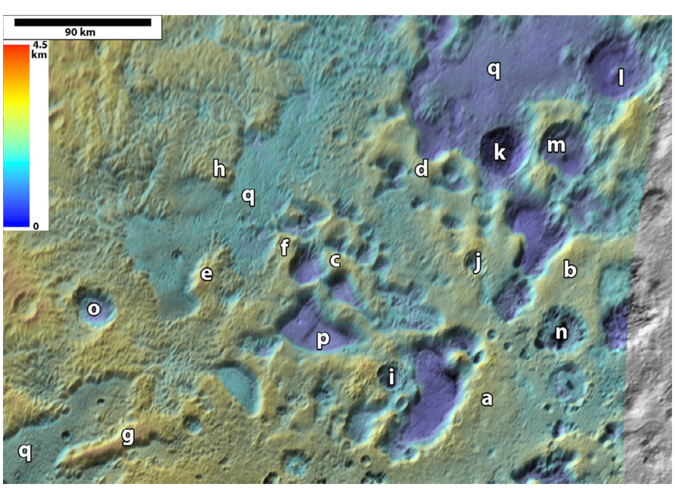

Fig. 4. Smooth uplands and pits terrain. North to top. Lambert conformal conic projection with standard parallels of 30°N and 50°N, with central meridian 210°E. Image centered at about 204.9°E. Region northwest of letters ‘g’ and ‘f’ is dissected terrain interpreted as glacially modified terrain. The rest of the map except for the extreme southeast corner is smooth-mantled terrain. See text for meaning of lettered features. See Fig. S2 for stereo anaglyph image and this image without letter labels. See Fig. 1 for location.

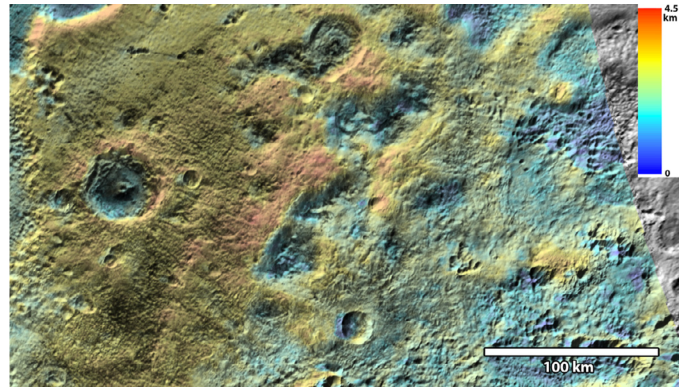

Fig. 5. Eroded smooth uplands terrain. North to top. Lambert conformal conic projection with standard parallels of 30°N and 50°N, with central meridian 210°E. Centered at 210.4°E and 40.6°N. Topography features broad ridges and depressions with 100 m scale rough surface interpreted to result from differential erosion of an ancient smooth mantle. Note several impact craters. See Fig. 1 for location.

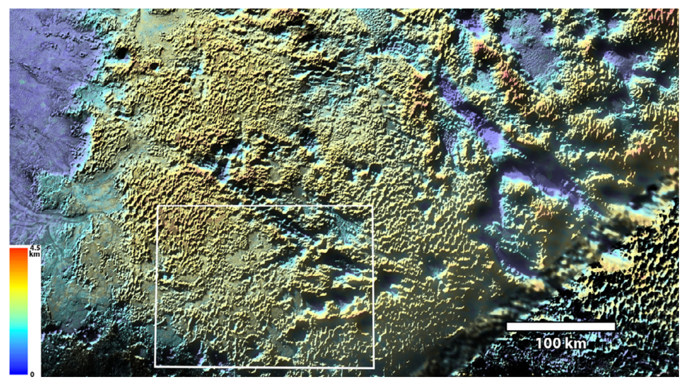

Fig 6. Bright pitted uplands and bladed terrain. Mercator projection. Centered at 3.0°N, 208.1°E. Bladed terrain occupies high portions of right third of image. Sputnik Planitia forms the left edge. The image histogram has been equalized to provide detail in both high and low albedo regions as well as shadows. The central part of the image is the bright pitted uplands, featuring polygonal ridges with a strong methane spectral signature interspersed with smooth lowlands with an N_2 spectral signature. Complexes of large pits (>10 km diameter) dominantly follow northeast to southwest tectonic lineations. See Fig. S5 for stereo anaglyph of bladed terrain and smooth-floored lowlands. See Fig. 1 for location. Box shows location of Fig. 7.

pits or lowlands. Complexes of smaller pits locally appear to have narrow, elevated rims (Figs. 11 and S6). Arrows in Fig. 11 indicate some of these elevated rims.

2.2.2. Possible pit complexes

This mapping unit distinguishes regions of pitting that are not sharply defined. It includes sparse pitting, depressions with rounded edges (possibly older, degraded pits), or depressions that are difficult to distinguish from other rough terrain (such as the cellular depressions on the bright pitted uplands, or structural troughs) (Fig. 2c).

2.2.3. Smooth-floored lowlands

These are relatively low-lying expanses with a generally smooth, nearly planar surface as resolved in 240 m/pixel imaging. Although they are relative depressions, the floor elevations span a ~1.5 km range within the smooth upland and pits terrain, although none appears to be lower than the ***SP*** surface (Figs. 4, 7, 12, and S2–S3). Crater floors and structural depressions, however, locally do reach elevations below ***SP*** (e.g., Fig. 4, location ‘k’). In the few locations where this unit is covered by imaging with resolution <120 m/pixel the surface is covered by 100–200 m pitting similar to that on ***SP***, which is of presumed sublimation origin because

Please cite this article as: A.D. Howard et al., Pluto: Pits and mantles on uplands north and east of Sputnik Planitia, Icarus (2017), http://dx.doi.org/10.1016/j.icarus.2017.02.027

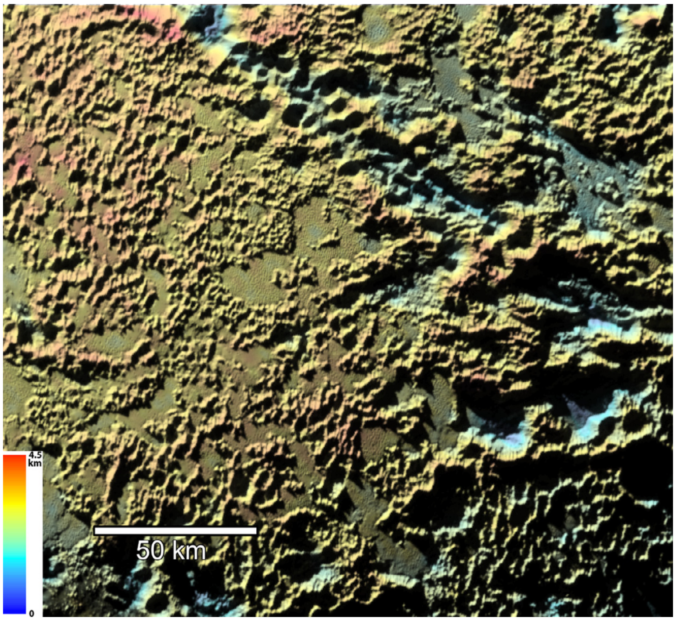

Fig. 7. Details of bright pitted uplands landforms with elevation cuing. Equirectangular projection centered at 0.5°S, 204.0°E. See Fig. S4 for stereo anaglyph image of this region. See Fig. 6 for location.

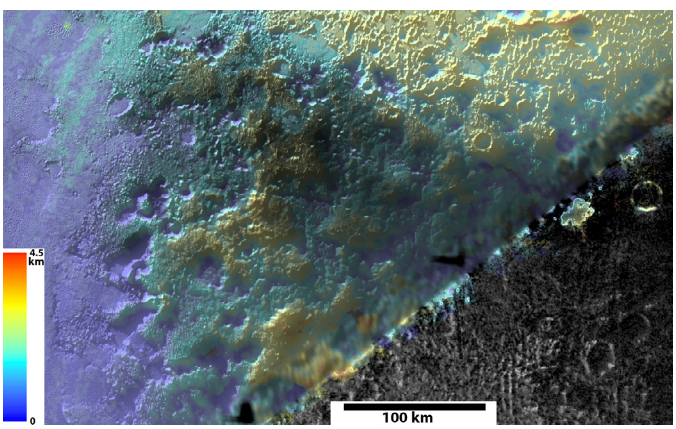

Fig. 8. The dark uplands terrain (Krun Macula). Mercator projection centered at 200.3°E, 10.0°S. Sputnik Planitia forms the left edge of the image. Dark coloration due to tholin mantling. Note the sharp albedo boundary with the bright pitted uplands at upper right. Lower right of image is from a stretched twilight image. Note the rough uplands interspersed with deep pits and troughs. Troughs along the western edge of the dark uplands region are floored with N_2-rich ices. See Fig. 1 for location.

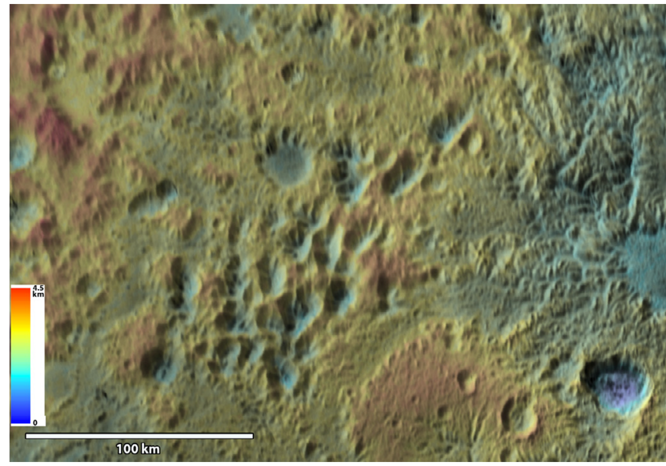

Fig. 9. Deeply pitted landscape between the northern rough uplands at upper left and the dissected terrain at lower right. Note that the pitting is partially aligned along a southwest–northeast tectonic lineation. The pitting is clearly incised below a pre-existing topographic surface. Lambert conformal conic projection with standard parallels of 30°N and 50°N, with central meridian 180°E. Centered at 190.2°E, 60.0°N. See Fig. S4 for stereo anaglyph of this region. See Fig. 1 for location.

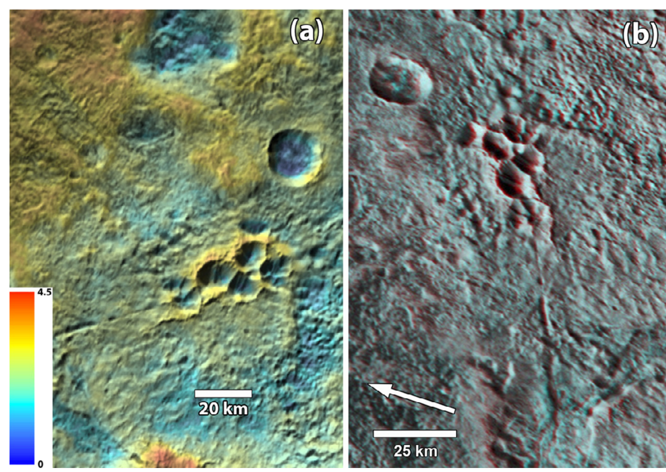

Fig. 10. Pits with elevated rims. (a) Elevation-cued image of pit cluster with elevated rims located along a tectonic lineation. Lambert conic projection with standard parallels of 30°N and 50°N, with central meridian 210°E. North is up. Image centered at 34.6°N, 207.9°E. (b) Stereo anaglyph image of same region. Arrow points north. See Fig 1 for location.

of the regular, concave morphology of the pits on volatile N_2 ices (Moore et al., 2017). This unit includes the modern glaciers on the western margin of the bright pitted uplands (Howard et al., 2017) as well as localized areas throughout all the mapped terrains.

2.2.4. Irregular-floored lowlands

This unit includes extensive lowland areas which, however, are somewhat less smooth than the smooth-floored lowlands or have an appreciable regional slope (Figs. 2b and 4, locations 'q'). Placement of many locations into the smooth versus irregular lowland category involves subjective evaluation and transitional relationships.

2.3. Relationships between landforms and surface composition

The LEISA imaging spectrometer as well as the MVIC visible-near-infrared scanning camera have mapped the spatial distribution of surface materials (including the non-volatile H_2O ice and dark mantles, and the volatile N_2 and CH_4 ices) with sufficient resolution to define strong relationships with the landforms discussed here (Grundy et al., 2016; Protopapa et al., 2017; Schmitt et al., 2017). Several compositional endmembers have been identified, *water ice*, N_2-*rich ices* with variable CO admixture and up to four percent solubility of CH_4, CH_4-*rich ices* with small amounts of N_2 and CO, and '*red materials*' with a diffuse spectral signature that are likely tholins produced by solar irradiation. Water ice forms the crustal bedrock but is extensively mantled by the other spectral units. The N_2: CH_4 binary phase diagram shows that composition intermediate between N_2-rich and CH_4-rich ices exists only as an intimate mixture (granular, or crystals within polycrystals) of N_2-rich and CH_4-rich ice phases, or as a stratification of these phases; (Schmitt et al., 2017), not as a molecular solid solution (Prokhvatilov and Yantsevich, 1983). The N_2-rich ices are dominantly very coarse grained, ranging from a few to tens of centimeters, whereas CH_4-rich ices are less than 1 mm in size (Protopapa et al., 2017).

Please cite this article as: A.D. Howard et al., Pluto: Pits and mantles on uplands north and east of Sputnik Planitia, Icarus (2017), http://dx.doi.org/10.1016/j.icarus.2017.02.027

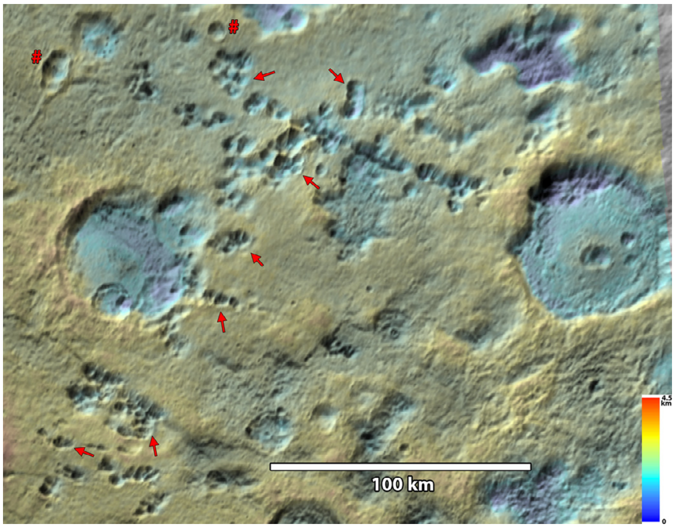

Fig. 11. Clusters of 1–3 km pits in eroded smooth uplands terrain. Most pits are aligned along structural lineations. Some of the pits (e.g., red arrows) have apparent raised rims. Pits marked with "#" are possibly impact craters. Lambert conformal conic projection with standard parallels of 30°N and 50°N, with central meridian 210°E, centered at 49.1°N, 210.8°E. See Fig. S6 for stereo anaglyph of this region. See Fig. 1 for location.

Several factors complicate relating surface mineralogy inferred from spectroscopy to landform features, their formation, and their bulk composition. Spectroscopy characterizes a surface layer than can be only microns thick for opaque minerals to possibly a few centimeters for translucent minerals and possibly decameters for N_2 ices on ***SP***. Surfaces subjected to erosion (e.g. by sublimation) may reflect bulk composition, but accumulated mantles may be unrelated to the substrate. Mantles may be deep accumulations that thickened over millions of years or may reflect seasonal volatile migrations (Protopapa et al., 2017; Schmitt et al., 2017). The spatial distribution of insolation over seasonal and long-term timescales is a primary control on patterns of volatile condensation and sublimation (Earle and Binzel, 2015; Bertrand and Forget, 2016; Earle et al., 2017; Stern et al., 2016). In addition, volatile distribution is affected by elevation (CH_4 tends to accumulate at high elevation and N_2 collects in relative depressions (Bertrand and Forget, 2016)), surface properties (e.g., albedo effects on temperature (Schmitt et al., 2017)), landform shape (e.g., cold traps on hill summits, radiation focusing in depressions (Howard and Moore, 2008; Howard et al., 2012; White et al., 2015; Moore et al., 2017)), and atmospheric circulation (Bertrand and Forget, 2016).

Nonetheless, observed relationships between inferred surface mineralogy and landform properties can mutually inform and constrain process interpretations. We therefore note consistent spectrally interpreted surface compositions associated with the landform units described below. The spectral characteristics of the portion of the uplands study area northeast of Sputnik Planitia are shown in Fig. 13, where red color indicated CH_4 ices, green N_2 ices, and blue water ice based on composition maps in Schmitt et al. (2017). Mixtures produce intermediate colors.

2.3.1. Landform associations

The uplands in the northern rough uplands display a strong CH_4 ice signature, as does most of the terrain north of 65–70°N (Protopapa et al., 2017; Schmitt et al., 2017). The broader depressions near the southern limit of this terrain, however, exhibit an N_2 ice signature (e.g., the lowlands in the south portion of Fig. 3). The dissected, smooth uplands and pits, and eroded smooth uplands terrains display a distinct pattern of uplands with CH_4 signature (locations 'b' in Fig. 13a) and lowlands dominated with N_2 and water ice surface mineralogy (locations 'a' in Fig. 13a). A stronger water ice signature occurs in some lowlands at the lower right of Fig. 13a (e.g., location 'f'). An exception occurs in lowland areas near ***SP*** in which CH_4 dominates (locations 'd' in Fig. 13a). Some larger degraded crater basins have rounded rims with a CH_4 ice signature (location 'c' in Fig. 13a), and deep, less degraded craters have floors rich in water ice ('g' in Fig. 13a). At the upper right of Fig. 13a some rounded ridges show a mix of CH_4 and water ice signatures (e.g., location 'i' in Fig. 13a). These terrains occur in a belt from about 35–65°N noted for relative abundance of N_2 ices (Protopapa et al., 2017; Schmitt et al., 2017). In the bright pitted uplands, N_2 dominates near ***SP*** as plateaus of ice draining as glaciers into ***SP*** (Howard et al., 2017; Moore et al., 2016) interspersed with reticulate ridges with a CH_4 signature. Farther eastward on the bright pitted uplands, isolated N_2-rich lowlands are surrounded by broad expanses of reticulate ridges with a strong CH_4 signature. The bladed terrain is dominated by CH_4 ice signature, with a few inliers of lowlands with an N_2 signature. The dark uplands are dominated by the spectral signature of 'red materials' (presumably organic materials similar to laboratory tholins). Pits, pit clusters, and troughs throughout the region have spectral signatures of methane on rims, but deeper pits and troughs have a strong water ice signature on their floors and lower slopes (e.g. locations 'e' in Fig. 13a).

3. Interpretation

3.1. Terminology

We use the term *cryovolcanic* as a generic term to cover a variety of modes of transfer of materials from the subsurface to the surface, primarily as a result of subsurface phase changes resulting from internal heat and pressure (e.g., Prockter, 2004; Moore et al., 2015). On Pluto likely materials are H_2O, N_2, and CH_4. Eruptive modes can include combinations of solids, gasses, and fluids in events ranging from explosive to slow gaseous emissions. When suggesting origin of features by cryovolcanism we specify as much as possible the likely mode of emplacement. We exclude sublimation, transport and condensation of volatiles from being cryovolcanism unless directly related to eruptions or subsurface heating.

3.2. Formation of pitted terrain

Relative depressions can form through a variety of mechanisms:

(1) Collapse through removal of material into subsurface voids, as in the funnel-like depressions that formed through draining of megaregolith into tensional fractures on the uplands surrounding Mars' Valles Marineris (Fig. 14). Large troughs with quasi-parallel walls are likely grabens, such as the linear depressions on the bright pitted uplands (Figs. 6, 7, and S3) and those incised into the dark uplands terrain (Fig. 8). Other mechanisms that might form subsurface voids are melting and draining of ices (especially N_2) and subsurface injection of ices followed by their subsequent removal or melting, both potentially leading to surface collapse.
(2) Differential sublimation of surface ices as is ascribed to form the small-scale pits on SP (e.g., Moore et al., 2017).
(3) Eruption of materials from the subsurface with or without local deposition, as occurs, e.g., for volcanic cinder cones and the tiger stripes of Enceladus.
(4) Impact cratering.
(5) Differential deposition of materials on ridges, as occurs in the cold-trapping of water ice on ridges on Callisto (Moore et al., 1999; Howard and Moore, 2008; White et al., 2014) and may possibly contribute to relief development around

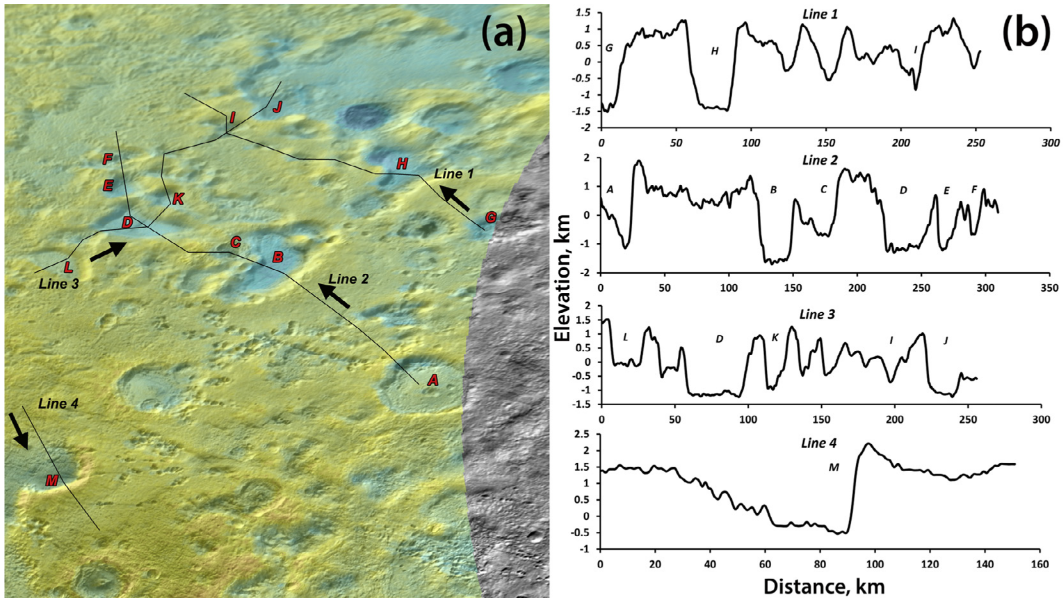

Fig. 12. Topographic profiles across pits and ridges in the smooth uplands and pits terrain. Equirectangular projection with north to top. Note that smooth pit floors (e.g., locations B, C, D, H, L, and M) have floor elevations ranging over about a 1.5 km elevation range. Smooth ridges between nearby pits are typically 8–12 km wide, but elevated rims southwest of depressions B, H, and M have concave slopes more than 20 km long leading from high, rounded ridges immediately adjacent to the depressions. Image centered at 53.3°N, 210.9°E. Arrows show direction of transect (left to right).

cellular pits on the bright pitted uplands and the bladed terrain (Moore et al., 2016, 2017).

Collapse of surface materials into subsurface voids appears to be the best explanation for most of the pitted terrain mapped in Fig. 2b. This interpretation is supported by the association between pits and tectonic lineations (Figs. 6–8, 11, and S3–S5), as well as the observation that most of the pit complexes are clearly indented below the surrounding terrain. Crustal tensional fracturing, possibly associated with global expansion due to progressive freezing of a subsurface water ocean is a likely mechanism for creation of subsurface voids encouraging surface collapse (Moore et al., 2016). Many of the fracture systems are radial to ***SP*** (Keane et al., 2016; Moore et al., 2016) and may be related to formation of ***SP*** by impact (Schenk et al., 2015; Johnson et al., 2016), subsurface ocean freezing (Hammond et al., 2016; Nimmo et al., 2016), and reorientation of ***SP*** (Keane et al., 2016; Nimmo et al., 2016). Some pit complexes, however, seem too extensive and involve too large a volume of missing material to be readily explained by tensional fracturing. The most obvious such case is the $\sim 90 \times 180$ km cluster of 15–20 km wide pits shown in Figs. 9 and S4. Although the pits are aligned along a tectonic lineation, there does not appear to be a convergence of fractures or evidence of a graben structure. Because the pits extend below the level of surrounding terrain, a constructional or eruptive origin seems unlikely as the dominant process. Removal of subsurface materials causing collapse of overlying deposits is a more likely explanation. The large flat-floored pits in the smooth mantled terrain (Figs. 4, 12, and S2) also seem unlikely to have formed simply by collapse along tensional fractures.

Sublimation of volatiles may contribute to the depth and width of some pits, but the deep, conical pits exposing water ice near along their steep lower walls and floors must have experienced subsurface removal of materials because of the non-volatility of water ice.

3.3. Origin of elevated pit rims

The striking elevated rims of the pits shown in Fig. 10, and possibly in Figs. 7 and S3, clearly record processes other than, or acting in addition to, collapse processes forming pits. The association of elevated-rim pits with structural lineations and their clustered pattern likely exclude formation by impact cratering. One possibility is that the rims are composed of cold-trapped volatiles, similar to enhancement of crater rims by deposition of re-precipitated water ice on Callisto (Moore et al., 1999, 2004; Howard and Moore, 2008; White et al., 2014). To have such height and localization to just a few pit complexes suggests some local enhancement of condensation—outgassing from the interior through pit floors is a possibility. Locally-enhanced N_2 and CH_4 sublimation due to a near-surface heat source (e.g. fluids upwelling along fractures) could result in elevated rims as the gases recondense on pit rims. Another possibility is emplacement as particulate rim deposits from gas-rich cryovolcanic eruptions similar to terrestrial cinder cones. The large central pit and narrow rims are unlike typical terrestrial cinder cones; the low gravity on Pluto, however, would permit wider dispersal of ballistic debris (McGetchin and Head, 1973). Explosive cryovolcanic formation remains a possibility, similar to calderas and maars on Earth. Explosive volcanism implies strong involvement of volatiles released in the subsurface; volatilization of N_2 is the most logical candidate for Pluto. Burr et al., (2009a) summarize several volcanic processes that can produce elevated rims surrounding central depressions. If sharp-crested elevated rims (e.g. as in Fig. 10) were formed by cold-trapped volatiles or erupted deposits, then the interior walls of the pits likely collapsed or retreated further after the material was deposited to account for the narrow divides.

An additional possibility is dome-like uplift of the surface followed by collapse of the center as intruding materials either drain or are melted or volatilized. Several terrestrial processes are potential analogs: (1). *Laccolithic intrusions*. Laccoliths are dome-like intrusions between layers of preexisting materials. They are injected from below and which elastically bend overlying layers (Gilbert, 1877; Hunt et al., 1953). Simple theoretical models predict the cross-sectional shape of laccoliths but not their absolute size (e.g., Turcotte and Schubert (2002)). The lid-stretching implied by uplift could result in extensional fracturing providing initiation points for pit development. The clustering of pits in Fig. 9 may

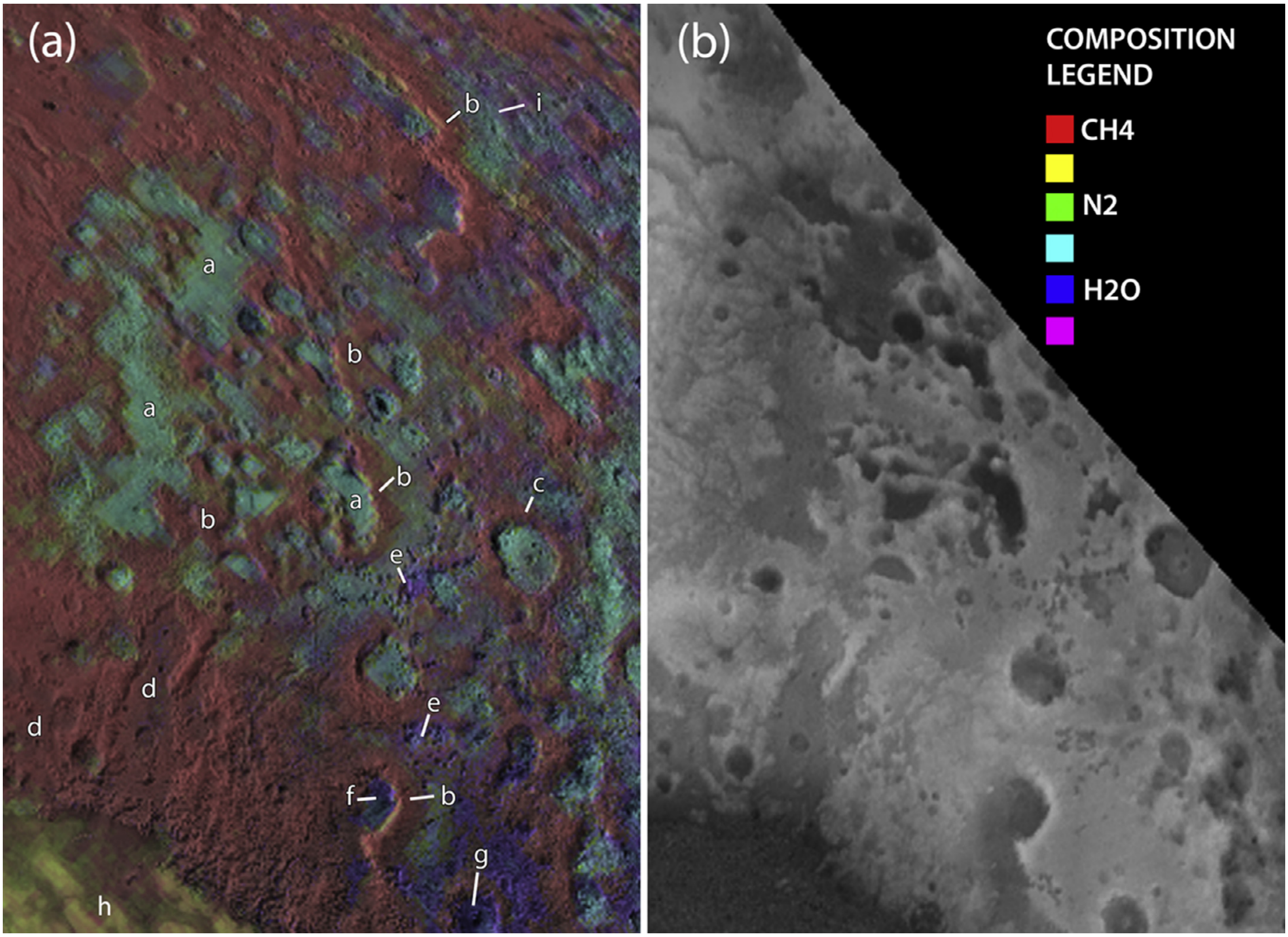

Fig 13. Surface composition and elevation maps. (a) Surface composition based upon interpretation of LEISA imaging spectrometer (Schmitt et al., 2017), overlaid on a MVIC visible image. Legend shows associations between colors and spectral indicators. Red band is CH_4-rich ices, blue band is water ice, and green band is N_2-rich ices, with other colors having intermediate compositions. For example, cyan coloration at locations 'a' is a mixture of N_2 and water ice spectral indications. Location 'h' is Sputnik Planitia, appearing yellow because of mixed N_2 and CH_4 ice signatures. See text for discussion of other lettered features. (b) Elevation map based on stereophotogrammetry. Elevation range from black to white is about 4.5 km. Elevation data do not cover the full extent of (a). See Fig. 1 for location. Orthographic projection with image width along lower axis about 680 km. See Fig. 1 for orientation of image. (For interpretation of the references to colour in this figure legend, the reader is referred to the web version of this article.)

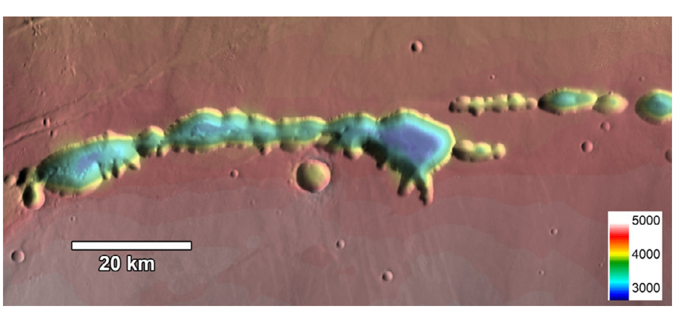

Fig. 14. Pit chains in the Tharsis region of Mars. Elevation-cued THEMIS daytime IR image centered at 3° 30′ S, 90° 14′ W. North to top.

be analogous to laccoliths being tightly clustered around one or more igneous stocks rather than being broadly distributed (Gilbert, 1877; Hunt et al., 1953). (2). *Diapirs.* This analog includes a variety of forms including domes and diapirs that are driven by a substrate layer that is deformable and less dense than overlying layers (Jackson et al., 1994, 1996; Jackson, 1995; Hudec and Jackson, 2007). On Earth this landform often involves salt intrusions, which can be triggered by thickness variations in the overlying layer as well as by compressional or extensional tectonics. Such a mechanism might not be viable on Pluto; although nitrogen-rich ice has low viscosity, it is denser than water and methane ices. CH_4 ice, however, has a significantly lower density than either N_2 or water ice, and if originating at depth, it would buoyantly rise, possibly forming diapirs. (3). *Pingos.* These are domical masses of ice formed in periglacial environments that structurally uplift surface sediment. *Open-system* pingos are formed by artesian pressure of groundwater beneath a frozen or impermeable carapace (Holmes et al., 1968; Yoshikawa et al., 1995; Sholz and Bauman, 1997). *Closed-system* pingos form in near-level terrain, often in drained lake basins due to top-down and inward freezing of wet sediment that injects water between the overlying and underlying permafrost (Walker et al., 1985; Mackay, 1988; Mackay and Burn, 2011; Jones et al., 2012). Only open-system pingos would be feasible on Pluto, because nitrogen ice contracts upon freezing. Fracturing associated with brittle failure of the overburden can expose the ice core to sublimation and melting, causing central depressions or lakes. Small domical structures with and without central pits on Mars have been attributed to being pingos (e.g. Soare et al., 2005;

Page and Murray, 2006; Soare et al., 2008; Burr et al., 2009b; de Pablo and Komatsu, 2009; Dundas and McEwen, 2010; Soare et al., 2014). All of these dome-forming mechanisms would presumably involve intrusion of nitrogen-rich ices and their sublimation upon exposure or their melting at depth. These intrusive mechanisms would, however, likely produce radial or circumferential fracturing, which is not evident at the elevated rim sites.

The less obvious circumferential ridges associated with some complexes of smaller pits (Figs. 11 and S6) may have formed by any of the mechanisms discussed above. Some of the apparent elevated ridges may, however, simply be rounded divides between a deep pit and a shallower adjacent pit.

Discussion of the broader elevated ridges surrounding depressions in the smooth uplands is presented in Section 3.5.2.

3.4. Formation of smooth lowlands

Most of the larger mapped smooth lowlands units (Figs. 4, 12, and S2) display a distinct N_2 signature in spectral mapping as well as water ice (Grundy et al., 2016; Protopapa et al., 2017; Schmitt et al., 2017), indicated by cyan coloring in Fig. 13. N_2 ice presence in relative depressions is compatible with origin by atmospheric condensation because such condensation favors low areas (e.g. ***SP***) (Bertrand and Forget, 2016). A position in depressions and a nearly planar surface likewise is compatible with lateral flow of the low-viscosity of N_2 ices, as occurs on ***SP***. At locations where the smooth lowlands are imaged at resolutions greater than 150 m/pixel, small-scale pitting is often observed, consistent with sublimation processes in N_2 ice deposits at least tens of meters thick (Moore et al., 2017). N_2 ice emplacement by upwelling, ponding, and freezing of N_2-rich ice from subsurface sources cannot be ruled out as a possible source.

The presence of a water ice signature in the smooth lowlands (Fig. 13) suggests a sub-pixel mixing of water ice with N_2 or a thin N_2-rich ice layer (a few to a few tens of cm) covering the H_2O ice bedrock. Unlike ***SP***, the smooth lowlands display subtle relief, such as the low scarp at ‘p’ in Fig. 4 and the small impact crater near ‘p’ . These topographic features would not persist if composed of thick N_2 ice (Moore et al., 2016, 2017; Umurhan et al., 2017). This relief suggests that a thin, possibly seasonal accumulation of N_2 ices on these lowlands either discontinuously mantles a water ice substrate or that the water ice is detectable through the thin remaining N_2 layer. The N_2 ice must be locally thick enough, however, to support sublimation pitting.

Like the pit walls, many of the scarp walls enclosing smooth lowlands have a near-planar texture and appear linear in profile (Figs. 4 and 12), suggesting that they have been subjected to mass wasting. One possible explanation for the steep walls is that the ices flooring the depressions have accumulated within pre-existing deep pits either by atmospheric condensation or upwelling. A difficulty with this scenario is that the steep-walled depressions in the smooth lowlands exceed 30 km from rim to rim. A simple pit of such dimensions would have to have been ten or more kilometers deep if the walls were at the angle of repose. Infilling of a complex of pits is more likely; the putative buried interior pit walls, however, would have had to be up to 1.5 km lower than an encompassing outer pit complex margin and organized so as to define an enclosing platform with uniformly sloping walls with a rounded planimetric form. Another possibility is that accumulation of the ices in depressions attacks and undermines the outer depression walls, gradually enlarging the depression. Because no slump deposits are identifiable covering the margins of the depression floors, slumping material would have to become incorporated into the accumulating ices or sublimated. If the depression-filling ices were formerly liquid (e.g., N_2 or water or a mixture), such an erosional attack of the lake margins is conceivable. This could occur if the lowlands were filled by cryovolcanic extrusions, melting or sublimating the pit walls. Examples of such cryovolcanic lateral (thermal) erosion occur on other Solar System objects. For example, boundary erosion and lake expansion by present or former methane-rich lakes has occurred in the sharp-edged depressions of Titan (Moore and Howard, 2010; Hayes, 2016; Birch et al., 2016). Water ice extrusions followed by withdrawal and collapse or near-surface intrusions and collapse have created depressions with steep lateral walls on Europa (e.g., Collins et al., 2000; Prockter and Schenk, 2005; Walker and Schmidt, 2015). The crenulated margins of Puach and Tuonela Planitia on Triton may have been eroded by cryovolcanic flows (Croft et al., 1995).

Another possibility is that climatic excursions might occasionally produce surface or shallow subsurface temperatures sufficient to melt the N_2 component of the depression floors (Stern et al., 2016). Some of large pits may be ancient impact basins that have been strongly modified (e.g., by widening and infilling).

3.5. Formation of irregular-floored lowlands

This unit is probably of diverse origin. Most areas, like the smooth lowlands, display a mixed N_2 and water ice spectral signature (e.g., locations ‘q’ in Fig. 4 and ‘a’ in Fig. 13). Some may be rougher or less level examples of the same materials and formation mechanisms as the smooth lowlands. Extensive patches of irregular-floored lowlands occur north and east of ***SP*** in or adjacent to the dissected terrain (Fig. 4, ‘q’). Some of these patches exceed 50 km in width and 100 km in length. Because of the probable origin of dissected terrain through glacial erosion and deposition, the associated lowlands may be glacial deposits, either unsorted till or outwash. The lowlands at locations ‘d’ in Fig. 13a constitute a broad, sloping plain rising 2 km from ***SP*** over a distance of about 150 km (Figs. 1 and 13b). This surface could be basement materials scraped clean of mantling units (discussed below) by glacial erosion.

3.6. Origin of upland mantles

The upland terrains (rough uplands, smooth uplands, and degraded smooth uplands) share large expanses of uplands having a strong CH_4 spectral signature and textures suggestive of deposited mantles and their possible subsequent erosional modification.

3.6.1. Rough uplands terrain

The highlands north of ***SP*** extending across the North Pole were imaged only at low resolution (~800 m/pixel). The irregular uplands are interrupted by depressions (Figs. 3 and S1). The larger of the depressions are flat-floored with N_2 ice signatures. The uplands are likely a dissected mantle of friable sediment up to 3 km in thickness, although layering is not distinguishable in the low-resolution images. At its southern end this mantle has been sculpted into the fluted terrain discussed in Howard et al., (2017), likely by glacial processes. Some flute-like dissection on the flanks of uplands extends to high latitudes, suggesting that glaciation may have affected much of this terrain unit. The rough uplands host a number of 20+ km diameter probable impact basins (Moore et al., 2016; Robbins et al., 2017) suggesting that the mantle is ancient. The origin of this extensive mantle is uncertain, but the primary geomorphic activity in this region during most of Pluto's history has dominantly involved erosion rather than deposition because of the rough surface texture. Because of the high relief and an apparently modest yield stress for methane ice (Eluszkiewicz and Stevenson, 1990; Yamashita et al., 2010) the uplands may be supported by water ice bedrock, although strong H_2O spectral signatures were not detected by LEISA.

The likely necessity for a large water ice component within the deposit to preserve the high relief and steep slopes is difficult to reconcile with its gradual accumulation as condensed volatiles. One alternative possibility is its emplacement as a locally thick accumulation of ***SP*** ejecta. The prominent troughs between the ridges are oriented roughly normal to the northern edge of the ***SP*** basin. The troughs could be sites where ejecta was rich in N_2 or CH_4 that has subsequently sublimated, leaving more water-ice rich deposits in relief and accounting for the apparent mass wasting and rough topography of the ridges.

3.6.2. Smooth uplands terrain

This terrain is one of the most enigmatic on Pluto. The rolling uplands comprise the smoothest upland unit on Pluto (locations ‘b’ and ‘c’ in Fig. 13a) and are interspersed with pits and flat-floored lowlands (locations ‘a’ in Fig. 13a). A strong geographic association exists between uplands and depressions, however. The relatively smooth-surface uplands rise up to 2 km above adjacent pits and depressions (Figs. 4, 12, and S2). The highest ridges in this unit are generally within 5–10 km of adjacent depressions (e.g., ‘a’–‘d’ in Fig. 4) but gradually decline in elevation beyond the ridge crests (i.e., with greater separation from the closest pits and depressions) (‘a’ and ‘b’ in Fig 4; Figs. 12 and S2). These relationships seem incompatible with a hypothesis that the pits and lowlands are simply incised into a pre-existing upland surface, leaving elevated uplands. Rather, it is likely that there is a genetic interrelationship between the uplands and pit/lowland formation. The relative smoothness of the uplands indicates their origin or modification by diffusive processes. Here we suggest that the uplands are a depositional mantle whose emplacement is strongly influenced by proximity to adjacent depressions.

One possibility is that the pits/depressions passively control deposition of the smooth mantles by affecting local atmospheric circulation (e.g., equivalent to land and sea breeze daily cycles) which might encourage condensation of methane-rich ices on nearby uplands in which the deposits on the depression floors have no direct role.

A stronger role of the nearby depressions would occur if they are the source of the upland mantles. Sublimation of N_2-rich ices from the flat-floored depressions might lead to condensation of the admixed, less-volatile CH_4 on surrounding uplands. Two issues, however, make this simple scenario implausible. The first is that methane-rich mantles also surround pits lacking the flat-floored depressions. The second is a mass-balance issue; the upland mantles are at least as voluminous as the pits, yet methane is a minor component of N_2-rich ices, so that the latter would have to be frequently resupplied, either though upwelling from below or atmospheric deposition.

Another possibility is that the pits and depressions are formed through long-lived energetic volcanic eruptions, in which ballistically-emplaced ejecta is deposited over distances up to tens of kilometers from the eruption sites. These deposits initially might be N_2-rich but readily sublimated, leaving a methane-rich residue. Unfortunately, image resolution over this region is unable to reveal any ballistically-emplaced blocks less than kilometer-scale.

Perhaps most likely is a gradual emplacement of the upland mantle from gaseous effusions from the subsurface emanating from the pits and depressions with the CH_4-rich component condensing on surrounding uplands. Liquid N_2 can dissolve a much larger amount of CH_4 (Prokhvatilov and Yantsevich, 1983) than can solid N_2, so that an extrusion and freezing of a *N_2-rich* liquid from the subsurface leaves a separate CH_4-rich phase that might contribute to upland mantles through sublimation, and recondensation on uplands.

The smooth uplands terrain and its common association with surrounding smooth-floored depressions have similarities to elevated-rim depressions in the polar regions of Titan (Birch et al., 2016). The Titan polar depressions are interpreted to be a combination of extant and dry methane lakes. The origin of their elevated rims through deposition by aeolian or sublimation/recondensation processes sourced from the adjacent pits has also been suggested (Birch et al., 2016).

3.6.3. Eroded smooth uplands terrain

This terrain is characterized by a broad, rolling topography at the scale of tens of kilometers but a rough, pitted texture at tens to hundreds of meters scale (Figs. 5, 11, and S6). We tentatively identify this as an older landscape formed in the same manner as smooth uplands terrain but subsequently roughened by sublimation pitting. In some, but not all, locations the higher uplands are associated with close proximity to adjacent depressions, such as the eastern edge of Fig. 12.

3.6.4. Bright pitted uplands

The high albedo of these uplands is likely due to recondensation of N_2 and CH_4 sublimated from ***SP*** (Moore et al., 2016), with accumulated N_2 driving return glacial flow from the highlands onto ***SP*** (Howard et al., 2017). The reticulate ridges with a strong CH4 signature are likely sculpted by solar-induced sublimation of the included depressions, possibly accompanied by cold-trap CH_4 accumulation on the ridges (Moore et al., 2016).

3.6.5. Dark uplands

The contrast in morphology between the bright pitted uplands, with its abundant N_2 flats and the CH_4-rich reticulate ridges suggests either that the low albedo and consequent higher temperatures created by the tholin mantle inhibits deposition of the N_2-rich icy flats (Schmitt et al., 2017) as well as inhibiting formation of the CH_4-rich cellular ridges and pits or, conversely, that volatile deposition on the bright pitted uplands (probably sourced from ***SP***) encourages their formation.

3.6.6. Bladed terrain

The prominent parallel, elevated ridges of bladed terrain (Figs. 5 and S5) are oriented predominantly north–south with about 4 km spacing, and display a dominant CH_4 spectral signature. Solar-induced sublimation of thick CH_4 deposits is likely involved in blade formation, as is discussed in a companion paper (Moore et al. in preparation) and in Moores et al., (2017).

3.7. Surface mineralogy and substrate composition

A limited suite of minerals/volatiles can form the substrate of the region north and east of ***SP***, specifically H_2O ice, N_2-rich ice, and CH_4-rich ice. CO can be admixed with N_2 ice, but it apparently has chemical and rheological properties similar to N_2 (Moore et al., 2016). Because of its low viscosity, N_2 (and CO) rapidly flow to form low-relief landforms if occurring in quantities more than a few meters thick, as on ***SP.*** Thick accumulations of N_2 comprise the active glaciers along the border between ***SP*** and the bright pitted uplands. The enclosed, smooth lowlands farther east on the bright pitted uplands (Figs. 6, 7, and S3) are likely also floored by an appreciable thickness of N_2, as suggested by their N_2 spectral signature and surficial sublimation pitting. The flat-floored depressions in the smooth uplands and pits terrain (both smooth and irregular variants) have an appreciable N_2 ice signature (Fig. 13). Hints of sublimation pitting in the highest-resolution images also suggest a volatile-rich surface. On the other hand, these broad depressions have greater local relief than SP, and locally they display low scarps and craters on their floors that could not long persist in thick N_2 ice (e.g., ‘p’ in Fig. 4). A water ice spectral signature also occurs in these depressions, suggesting that water ice may shallowly underlie the basins. Similar concerns about the substrate composition occur for the lowlands at the south end of the northern rough uplands that display an N_2 spectral signature and apparent sublimation texturing but host a number of sharply defined craters.

The rheologic strength of CH_4-rich ice is uncertain because of conflicting experimental measurements (Eluszkiewicz and Stevenson, 1990; Yamashita et al., 2010) and a strong strength dependency on grain size (Howard et al., 2017; Umurhan et al., 2017). CH_4 ices dominate the spectra of all the landforms interpreted to be mantling deposits, the northern rough uplands (Fig. 3), the rounded ridges of the smooth uplands and pits (Fig. 4) and eroded smooth uplands (Fig. 5), the reticulate ridges of the bright pitted uplands (Fig. 7), and the bladed terrain (Fig. S5). Some scarps in these uplands are taller than 1 km and possibly as steep as 30°. The intricate pitting on the reticulate ridges, the bladed terrain, and the moderate pitting of the eroded smooth uplands are all suggestive of the involvement of sublimation processes, which would not occur if the mantles were dominated by non-volatile water ice.

Schmitt et al., (2017) suggest that seasonal condensation of a N_2-rich ices containing a small component of CH_4 might result, upon subsequent sublimation, in a surface cap CH_4-rich ice because of its lower volatility. This CH_4 cap might be underlain by residual N_2-rich ice. By extension, in locations of net long-term volatile deposition, a layered CH_4-rich/N_2-rich deposit might accumulate. The high relief of the most of the mantled terrains discussed here (northern rough uplands, bright pitted uplands, and bladed terrain) preclude appreciable N_2 in the near-surface substrate due to its low strength. The mantles on the smooth uplands and pits and eroded smooth uplands might, however, have achieved their broadly rounded divides through diffusive mass wasting because of a small component of interlayered N_2-rich ices, analogous to solifluction creep in terrestrial periglacial environments.

Water ice clearly underlies the entire region at some depth. A moderately strong water ice spectral signature occurs on both the smooth- and irregular-floored lowlands in the dissected, smooth uplands and eroded smooth uplands terrains (Figs. 4, 13, and S2). These units host a number of impact craters, suggesting a rigid substrate. Although these units tend to have low relief and are nearly planar over tens of km, individual lowlands occur over an elevation range of more than 1.5 km, and nearby lowlands can lie at very different elevations (Figs. 4, 13, and S2). Cryovolcanic resurfacing through multiple events might explain these characteristics. Glacial scour in the dissected terrains may have locally exposed these water ice platforms (e.g., in the upper left of Fig. 4 and the sloping near-planar surfaces at ‘d’ in Fig. 13).

4. Age relationships

The rough mantled terrain is likely the oldest highlands depositional unit to the north and east of ***SP***. It comprises one of the highly cratered units on Pluto (although erosion of the mantle may be exhuming some older craters) (Moore et al., 2016; Robbins et al., 2017). It has been affected by structural deformation (the linear depressions) and general surface erosion to form the rough surface. At its southern end (and possibly its western edge as well) it has been eroded into fluted terrain, probably by glaciation (Howard et al., 2017).

Large impact basins also occur within the eroded smooth uplands, smooth uplands, and dissected terrains (Moore et al., 2016; Robbins et al., 2017), indicating an ancient surface that has been modestly affected by subsequent erosional and depositional processes. Of these units, we infer that the effective surface ages decrease in the order listed. Mantle deposition has clearly ceased on the degraded smooth uplands terrain, and it has been strongly modified by sublimation pitting of the methane-rich mantling deposit. The smooth uplands terrain is only modestly affected by sublimation pitting, although a few impact craters superimpose this unit, such as the 18 km diameter crater at ‘j’ in Fig. 4, which has an obvious ejecta blanket. In general, however, superposition recognition of craters is difficult to assess on these terrains. The deep 32 km diameter crater at ‘k’ in Fig. 4 is clearly younger than the Smooth and Irregular Lowlands on which it sits, but its age relationship to the upland mantles is uncertain. Craters ‘l’, ‘m’, and ‘n’ appear to be older than the adjacent smooth mantles, but their interiors are only modestly affected by post-impact processes. Crater ‘o’ appears to have been affected by the processes creating the dissected terrain. It is nearly impossible to determine age relationships for craters <10 km in diameter or even to distinguish them from pits. Several <10 km round depressions occur on the Smooth and Irregular lowlands in this region (e.g., in Fig. 4) that are likely impact craters. Despite these uncertainties, however, all of these terrain units have been modified by scattered impacts of km to tens of km scale, placing them in Pluto’s middle age (Robbins et al., 2017; Singer et al., 2016).

The processes (probably N_2 glaciation) creating dissected terrain appear to be younger than the formation of the smooth mantled terrain. The uplands near ‘h’ in Fig. 4 that have been dissected retain the broadly rounded aspect at the scale of tens of kilometers that characterize the smooth mantled terrain (e. g., at ‘a–d’). The broad hill at ‘e’ also appears to be an example of modification of smooth uplands, as does ‘f’ . The smooth-topped linear hill at ‘g’ may be an example of a smooth mantled hill being surrounded by dissected terrain and may have been a nunatak protruding above glacial ice. The terrace on the north side of this ridge suggests that the N_2 ice was less than 1.5 km thick.

Impact craters are even more difficult to recognize on the Bright Pitted Uplands and the dark uplands terrains because of the rough texturing and extensive pitting. A few larger impact craters have been mapped here (Moore et al., 2016; Robbins et al., 2017), but their age relationship to the pits and reticulate terrain is uncertain. The N_2-rich ices of the smooth lowlands in the bright pitted uplands (including the active glaciers) appear to be free of craters, suggesting a surface age <10 Ma (Moore et al., 2016), although the deposits may be more ancient because of the low viscosity of N_2 ice, which would rapidly heal depressions (Moore et al., 2017). The high albedo of the bright pitted uplands suggests recent and possibly ongoing deposition of ices, and it would be consistent with continuing evolution of the landforms in this region.

5. Conclusions

The regions north and east of Sputnik Planitia provide evidence of the long-term evolution of Pluto. Particularly to the north and northeast, abundant craters indicate relatively modest modification of the landscape since the cessation of heavy bombardment. The northern rough uplands are mantled by a kilometers-thick mantle that was emplaced early in Pluto’s history and has been eroded to form the disordered, rough topography. Some of the larger craters at low relative elevation may be exhumed. Uplands at the southern end of this terrain have been dissected into fluted terrain, likely through nitrogen glaciation (Howard et al., 2017).

The formation of the smooth uplands and pits terrain has possibly involved cryovolcanism or localized volatile release and deposition, with the broad uplands being mantled by deposits sourced from adjacent conical and flat-floored depressions through either low-power explosive emplacement or through long-term accumulation of deposits from gaseous emanations and volatile condensation.

The eroded smooth uplands appears to be an older terrain formed by processes similar to the smooth uplands and pits terrain but modified by sublimation pitting. The younger bright pitted uplands and bladed terrains are likely related to condensation of N_2 and CH_4 derived from sublimation from ***SP*** accompanied by return N_2 glacial flow onto ***SP*** discussed in Howard et al., (2017) and solar-induced CH_4 sublimation and possible cold-trap condensation forming the reticulate ridges and enclosed depressions (Moore et al., 2016, 2017).

Pits and depressions are widespread in the regions north and east of Sputnik Planitia. Many are conical in form and aligned along tectonic lineations, suggesting removal of material to the subsurface due to tensional crustal fracturing, perhaps related to freezing of a primordial subsurface water ocean (Moore et al., 2016). More extensive pit complexes may have required broad subsurface collapse. Flat-floored depressions are widespread in the mapped region. Most display a mixed N_2 water ice spectral signature. Some of these depressions are involved in the active glaciation east of Sputnik Planitia. Where observed in higher-resolution imaging the surface of these depressions displays extensive pitting at the scale of 100–300 m, which is interpreted to result from sublimation (Moore et al., 2017). The relatively planar surface of these depressions suggests emplacement by fluid flows containing or dominated by water ice, or possibly resurfacing by low-viscosity, plastically deforming N_2-rich solids. Both the presence of sublimation pitting and the nearly level surfaces suggest that the more areally extensive, flat-floored depressions are mantled with N_2 ice, but the water ice signature coupled with low scarps and at least one impact crater suggest that water ice provides some rigidity. Most of the elevated terrain in this region has a strong spectral signature of methane (Grundy et al., 2016; Protopapa et al., 2017; Schmitt et al., 2017). This area includes the Rough Uplands, the ridges of the smooth uplands and pits terrain, the reticulate ridges of the bright pitted uplands, and the bladed terrain. Atmospheric condensation of methane is favored at higher elevations (Bertrand and Forget, 2016; Grundy et al., 2016). It is unclear whether the methane is a seasonal frost or an important component of the upland mantles. The rheologic strength of methane is uncertain (Moore et al., 2017), but it may be unable to support appreciable relief over geologic timescales. Little spectral signature of the structurally rigid, low-volatility water ice is seen in the mantles (Grundy et al., 2016; Protopapa et al., 2017; Schmitt et al., 2017), leaving the composition of mantling deposits uncertain.

Acknowledgment

This work was supported by NASA's New Horizons project. We are particularly grateful for detailed and helpful comments by Rossman Irwin and an anonymous reviewer.

Supplementary materials

Supplementary material associated with this article can be found, in the online version, at doi:10.1016/j.icarus.2017.02.027.

References

Bertrand, T., Forget, F., 2016. Observed glacier and volatile distribution on Pluto from atmosphere-topography processes. Nature 540, 86–89. doi:10.1038/nature19337.
Birch, S.P.D., Hayes, A.G., Dietrich, W.E., Howard, A.D., Bristow, C.S., Malaska, M.J., Moore, J.M., Mastrogiuseppe, M., Hofgartner, J.D., Williams, D.A., White, O.L., Soderblom, J.M., Barnes, J.W., Turtle, E.P., Lunine, J.I., Wood, C.A., Neish, C.D., Kirk, R.L., Stofan, E.R., Lorenz, R.D., Lopes, R.M.C., 2016. Geomorphologic mapping of Titan's polar terrains: constraining surface processes and landscape evolution. Icarus doi:10.1016/j.icarus.2016.08.003.
Burr, D.M., Bruno, B.C., Lanagan, P.D., Glaze, L.S., Jaeger, W.L., Soare, R.J., Wan Bun Tseung, J.-M., Skinner, J.A., Baloga, S.M., 2009a. Mesoscale raised rim depressions (MRRDs) on Earth: a review of the characteristics, processes, and spatial distributions of analogs for Mars. Planet. Space Sci. 57 (5-6), 579–596.
Burr, D.M., Tanaka, K.L., Yoshikawa, K., 2009b. Pingos on Earth and Mars. Planet. Space Sci. 57 (5-6), 541–555.
Collins, G.C., Head, J.W.III, Pappalardo, R.T., Spaun, N.A., 2000. Evaluation of models for the formation of chotic terrain on Europa. J. Geophys. Res, 105 (E1), 1709–1716.
Croft, S.K., Kargel, J.S., Kirk, R.L., Moore, J.M., Schenk, P.M., Strom, R.G., 1995. The geology of Triton. In: Cruickshank, R.P., Mattherws, M.S., Schumann, A.M. (Eds.), Neptune and Triton. University of Arizona Press, Tucson, USA, pp. 879–947.
de Pablo, M.A., Komatsu, G., 2009. Possible Pingo fields in the Utobia basin, Mars: geological and climatical implications. Icarus 199, 49–74.
Dundas, C.M., McEwen, A.S., 2010. An assessment of evidence for pingos on Mars using HiRISE. Icarus 205 (1), 244–258.
Earle, A.M., Binzel, R.P., 2015. Pluto's insolation history: latitudinal variation and effects on atmospheric pressure. Icarus 250, 405–412.
Earle, A.M., Binzel, R.P., Young, E.F., Stern, S.A., Ennico, K., Grundy, W.M., Olkin, C.B., Weaver, H. Geology and Geophysics Imaging Team, 2017. Long-term surface temperature modeling of Pluto. Icarus 287, 37–46. doi: do.1016/j.icarus.2016.09.036
Eluszkiewicz, J., Stevenson, D.J., 1990. Rheology of solid methane and nitrogen: applications to Triton. Geophys. Res. Lett. 17 (10), 1753–1756.
Gilbert, G.K., 1877. Report on the Geology of the Henry Mountains [Utah]. U. S. Geographical and Geological Survey of the Rocky Mountains Region, Washington.
Grundy, W.M., Binzel, R.P., Buratti, B.J., Cook, J.C., Cruikshank, D.P., Dalle Ore, C.M., Earle, A.M., Ennico, K., Howett, C.J.A., Lunsford, A.W., Olkin, C.B., Parker, A.H., Philippe, S., Protopapa, S., Reuter, D.C., Schmitt, B., Singer, K.N., Verbiscer, A.J., Beyer, R.A., Buie, M.W., Cheng, A.F., Jennings, D.E., Linscott, I.R., Parker, J.W., Schenk, P.M., Spencer, J.R., Stansberry, J.A., Stern, L.A., Throop, H.B., Tsang, C.C.C., Weaver, H.A., Young, L.A., 2016. Surface compositions across Pluto and Charon. Science 351 (6279), 1283. aad9189. doi: 1210.1016/science.aad9189
Hamilton, D.P., Stern, S.A., Moore, J.M., et al., 2016. The rapid formation of Sputnik Planitia early in Pluto's history. Nature 540, 97–99. doi:10.1028/nature20586.
Hammond, N.P., Barr, A.C., Parmentier, E.M., 2016. Recent tectonic activity on Pluto driven by phase changes in the ice shell. Geophys. Res. Lett. 43, 6775–6782 doi:6710.1002/2016GL069220.
Hayes, A.G., 2016. The lakes and seas of Titan. Ann. Rev. Earth Planet. Sci. 44, 57–83 doi:10/1146/annurev-earth-060115-012247.
Holmes, G.W., Hopkins, D.M., Foster, H.L., 1968. Pingos in Central Alaska. U. S. Geol. Surv. Bull. H1–H40 1241-H.
Howard, A.D., Moore, J.M., Umurhan, O.M., White, O.L., Anderson, R.S., McKinnon, W.B., Spencer, J.R., Schenk, P.M., Beyer, R.A., Stern, S.A., Ennico, K., Olkin, C.B., Weaver, H.A., Young, L.A., the New Horizons Science Team, 2017. Present and past glaciation on Pluto. Icarus 287, 287–300. doi:10.1016/j.icarus.2016.1007.1006.
Howard, A.D., Moore, J.M., 2008. Sublimation-driven erosion on Callisto: a landform simulation model test. Geophys. Res. Lett. 35, L03203. doi: 03210.01029/02007GL032618
Howard, A.D., Moore, J.M., Schenk, P.M., White, O.L., Spencer, J., 2012. Sublimation-driven erosion on Hyperion: topographic analysis and landform simulation model tests. Icarus 220 (1), 268–276.
Hudec, M.R., Jackson, M.P.A., 2007. Terra Inferma: understanding salt tectonics. Earth Sci. Rev. 82, 1–28.
Hunt, C.B., Averitt, P., Miller, R.L., 1953. Geology and geography of the Henry mountains region, Utah. U. S. Geological Survey Professional Paper, P0228, 234.
Jackson, M.P.A., 1995. Retrospective salt tectonics. In: Jackson, M.P.A., Roberts, D.G., Snelson, S. (Eds.), Salt Tectonics: A Global Perspective. American Association of Petroleum Geologists, Tulsa, OK, USA, pp. 1–28.
Jackson, M.P.A., Roberts, D.G., Snelson, S (Eds.), 1996, Salt Tectonics: A Global Perspective. American Association of Petroleum Geologists AAPG Memoir 65.
Jackson, M.P.A., Vendeville, B.C., Schultz-Ela, D.D., 1994. Structural dynamics of salt systems. Ann. Rev. Earth Planet. Sci. 22, 93–117.
Johnson, B.C., Bowling, T.J., Trowbridge, A.J., Freed, A.M., 2016. Formation of Sputnik Planum basin and the thickness of Pluto's subsurface ocean. Geophys. Res. Lett. 43 (10). 068-010-077. doi: 010.1002/2016GL070694
Jones, B.M., Grosse, G., Hinkel, K.M., Arp, C.D., Walker, S., Beck, R.A., Galloway, J.P., 2012. Assessment of pingo distribution and morphometry using an IfSAR derived digital surface model, western Arctic Coastal Plain, Northern Alaska. Geomorphology 138, 1–14.
Keane, J.T., Matsuyama, I., Kamata, S., Steckloff, J.K., 2016. Reorientation and faulting of Pluto due to volatile loading within Sputnik Planitia. Nature 540, 90–93. doi:10.1038/nature20120.
Mackay, J.R., 1988. Pingo growth and collapse, Tuktoyaktuk Peninsula Area, Western Arctic Coast, Canada: a long-term field study. Geogr. Phys. Quat. 52 (3), 271–323.
Mackay, J.R., Burn, C.R., 2011. A century (1910-2008) of change in a collapsing Pingo, Parry Peninsula, Western Arctic Coast, Canada. Permafrost Periglacial Process. 22, 266–272.
McGetchin, T.R., Head, J.W., 1973. Lunar cinder cones. Science 180 (4081), 68–72. doi:10.1126/science.1180.4081.1168.
Moore, J.M., et al., 2004. Callisto. In: Baginal, F., Dowling, T., McKinnon, W. (Eds.), Jupiter, the Planet, Satellites, and Magnetosphere. Cambridge University Press, Cambridge, pp. 397–426.
Moore, J.M., Howard, A.D., 2010. Are the basins of Titan's Hotei Regio and Tui Regio sites of former low latitude seas? Geophys. Res. Lett. 37, L22205. doi:10.1029/2010GL045234.

Moore, J.M, Howard, A.D., Schenk, P.M., McKinnon, W.B., Pappalardo, R.T., Ewing, R.C., Bierhaus, E.B., Bray, V.J., Spencer, J.R., Binzel, R.P., Buratti, B., Grundy, W.M., Olkin, C.B., Reitsema, H.J., Reuter, D.C., Stern, S.A., Weaver, H., Young, L.A., Beyer, R.A., 2015. Geology before Pluto: pre-encounter considerations. Icarus 246, 65–81.

Moore, J.M., Howard, A.D., Umurhan, O.M., White, O.L., Schenk, P.M., Beyer, R.A., McKinnon, W.B., Spencer, J.R., Grundy, W.M., Lauer, T.R., Nimmo, F., Young, L.A., Stern, L.A., Weaver, H.A., Olkin, C.B., Ennico, K.the New Horizons Science Team, 2017. Sublimation as a landform-shaping process on Pluto. Icarus 287, 320–333. doi:10.1015/j.icarus.2016.1008.1025.

Moore, J.M., McKinnon, W.B., Spencer, J.R., Howard, A.D., Schenk, P.M., Beyer, R.A., Nimmo, F., Singer, K.N., Umurhan, O.M., White, O.L., Stern, S.A., Ennico, K., Olkin, C.B., Weaver, H.A., Young, L.A., Binzel, R.P., Buie, M.W., Buratti, B.J., Cheng, A.F., Cruikshank, D.P., Grundy, W.M., Linscott, I.R., Reitsema, H.J., Reuter, D.C., Showalter, M.R., Bray, V.J., Chavez, C.L., Howett, C.J.A., Lauer, T.R., Lisse, C.M., Parker, A.H., Porter, S.B., Robbins, S.J., Runyon, K., Stryk, T., Throop, H.B., Tsang, C.C.C., Verbiscer, A.J., Zangari, A., Chaikin, A.L., Wilhelms, D.E., New Horizons Science Team, 2016. The geology of Pluto and Charon through the eyes of New Horizons. Science 351 (6279), 1284–1293.

Moore, J.M., Asphaug, E., Morrison, D., Klemaszewski, J.E., Sullivan, R.J., Chaung, F., Greeley, R., Bender, K.C., Geissler, P.E., Chapman, C.R., Helfenstein, P., Pilcher, C.B., Kirk, R.L., Giese, B., Spencer, J.R., 1999. Mass movement and landform degradation on the icy Galilean satellites: results from the Galileo nominal mission. Icarus 140, 294–312.

Moores, J.E., Smith, C.L., Toigo, A.D., Guzewith, S.D., 2017. Penitentes as the origin of the bladed terrain of Tartarus Dorsa on Pluto. Nature 541, 188–190.

Nimmo, F., Hamilton, D.P., McKinnon, W.B., Schenk, P.M., et al., 2016. Reorientation of Sputnik Planitia implies a subsurface ocean on Pluto. Nature 540, 94-86. doi:10.1038/nature20148.

Page, D., Murray, J., 2006. Stratigraphical and morphological evidence for pingo genesis in the Cerberus plains. Icarus 183 (1), 46–54.

Prokhvatilov, A.I., Yantsevich, L.D., 1983. X-ray investigation of the equilibrium phase diagram of CH_4-N_2 solid mixtures. Sov. J. Low Temp. Phys. 9, 94–98.

Prockter, L.M., 2004. Ice volcanism on Jupiter's moons and beyond. In: Lopes, R.M.C., Gregg, T.K.P. (Eds.), Volcanic Worlds: Exploring the Solar System's Volcanoes. Springer-Verlag, Berlin, pp. 145–177.

Prockter, L., Schenk, P., 2005. Origin and evolution of Castalia Macula, an anomalous young depression on Europa. Icarus 177, 305–326.

Protopapa, S., Grundy, W.M., Reuter, D.C., Hamilton, D.P., Dalle Ore, C.M., Cook, J.C., Cruikshank, D.P., Schmitt, B., Plilippe, S., Quico, E., Binzel, R.P, Earle, A.M., Ennico, K., Howett, C.J.A., Lunsford, A.W., Olkin, C.B., Parker, A., Singer, K.N., Stern, A., Verbiscer, A.J., Weaver, H.A., Young, L.A.the New Horizons Science Team, 2017. Pluto's global surface composition through pixel-by-pixel Hapke modeling of New Horizons Ralph/LEISA data. Icarus 287, 218–228. doi:10.1016/j.icarus.2016.1011.1028.

Robbins, S.J., Singer, K.N., Bray, V.J., Schenk, P.M., Lauer, T.R., Weaver, H.A., Runyon, K., McKinnon, W.B., Beyer, R.A., Porter, S., White, O.L., Hofgartner, J.D., Zangari, A.M., Moore, J.M., Young, L.A., Spencer, J.R., Binzel, R.P., Buie, M.W., Buratti, B.J., Cheng, A.F., Grundy, W.M., Linscott, I.R., Reitsema, H.J., Reuter, D.C., Showalter, M.R., Tyler, G.L., Olkin, C.B., Ennico, K.S., Stern, S.A., New Horizons LORRI and MVIC Instrument Teams, 2017. Craters of the Pluto-Charon system. Icarus 287, 187–206. doi:10.1015/j.icarus.2016.1009.1027.

Schenk, P.M., McKinnon, W., Moore, J.M., Nimmo, F., Stern, S.A., Weaver, H., Ennico, K., Olkin, C.B., Young, L.A., 2015. A large impact origin for Sputnik Planum and surrounding terrains, Pluto? In: American Astronomical Society Division of Planetary Science Meeting #47, p. id.200.06.

Schmitt, B., Philippe, S., Grundy, W.M., Reuter, D.C., Côte, R., Quirico, E., Protopapa, S., Young, L.A., Binzel, R.P., Cook, J.C., Cruikshank, D.P., Dalle Ore, C.M., Earale, A.M., Ennico, K., Howett, C.J.A., Jennings, E.E., Linscott, I.R., Lunsford, A.W., Olkin, C.B., Parker, A.H., Parker, J.Wm., Singer, K.N., Spencer, J.R., Stansberry, J.A., Stern, S.A., Tsang, C.C.C., Verbiscer, A.J., Weaver, H.A., the New Horizons Science Team, 2017. Physical state and distribution of materials at the surface of Pluto from New Horizons LEISA imaging spectrometer. Icarus 287, 229–260. doi:10.1016/j.icarus.2016.12.025.

Sholz, H., Bauman, M., 1997. An 'open system pingo' near Kangerlussuaq (Søndre Strømfjord), West Greenland. Geol. Greenland Surv. Bull. 176, 104–108.

Singer, K.N., McKinnon, W.B., Robbins, S.J., Schenk, P.M., et al., 2016. Craters on Pluto and Charon – Surface ages and impactor populations. Lunar Planet. Sci. Conf. 47, 2310 Abstract.

Soare, R.J., Burr, D.M., Wan Bun Tseung, J.M., 2005. Possible pingos and a periglacial landscape in northwest Utopia Planitia. Icarus 174 (2), 373–382.

Soare, R.J., Conway, S.J., Dohm, J.M., El-Maarry, M.R., 2014. Possible open-system (hydraulic) pingos in and around the Argyre impact region of Mars. Earth Planet. Sci. Lett. 398, 25–36.

Soare, R.J., Osinski, G.R., Costard, F., 2008. Recent, Late Amazonian Pingos, ice-rich landscapes and periglacial ponding in Utopia and Western Elysium Planitia, Mars, Lunar planet. In: Science Conference, p. 1315. Abstr..

Stern, S.A., Enniko, K., Mckinnon, W.B., Moore, J.M., Olkin, C.B., Spencer, J.R., Weaver, H.A., Young, L.A., Binzel, R.P., Earle, A.M., Singer, K.N., 2016. Past epochs of significantly higher pressure atmospheres on Pluto. Icarus 287, 47–53. doi:10.1016/j.icarus.2016.1011.1022.

Turcotte, D.L., Schubert, G., 2002. Geodynamics. Cambridge University Press, Cambridge.

Umurhan, O.M., Howard, A.D., Moore, J.M., Earle, A.M., Binzel, R.P., Stern, S.A., Schenk, P.M., Beyer, R.A., White, O.L., Nimmo, F., McKinnon, W.B., Ennico, K., Olkin, C.B., Weaver, H.A., Young, L.A., 2017. Modeling glacial flow on and onto Pluto's Sputnik Planum. Icarus 287, 301–319. doi:10.1016/j.icarus.2017.01.017.

Walker, C.C., Schmidt, B.E., 2015. Ice collapse over trapped water bodies on Enceladus and Europa. Geophys. Res. Lett. 42, 712–719. doi:10.1002/2014GL062405.

Walker, D.A., Walker, M.D., Everett, K.R., Webber, P.J., 1985. Pingos of the Prudhoe Bay Region, Alaska. Arc. Alp. Res. 17 (3), 321–336.

White, O.L., Moore, J.M., McKinnon, W.B., Spencer, J.R., Howard, A.D., Schenk, P.M., Beyer, R.A., Nimmo, F., Singer, K.N., Umurhan, O.M., Stern, S.A., Ennico, K., Olkin, C.B., Weaver, H.A., Cheng, A.F., Bertrand, T., Binzel, R.P., Earle, A.M., Grundy, W.M., Laurer, T.R., Protopapa, S., Robbins, S.J., Schmitt, B., the New Horizons Science Team, 2017. Geological mapping of Sputnik Planum on Pluto. Icarus 287, 261–286. doi:10.1016/j.icarus.2017.01.011.

White, O.L., Umurhan, O.M., Howard, A.D., Moore, M.J., 2014. Modeling of sublimation-driven erosion and ice pinnacle formation on Callisto. Geological Society of America Annual Meeting, 2014, Vancouver, B.C., Canada, Paper 84–85.

White, O.L., Umurhan, O.M., Moore, J.M., Howard, A.D., 2015. Modeling of ice pinnacle formation on Callisto. J. Geophys. Res. Planets 121, 21–45. doi:10.1002/2015JE004846.

Yamashita, Y., Kato, M., Arakawa, M., 2010. Experimental study on the rheological properties of polycrystalline solid nitrogen and methane: implications for tectonic processes on Triton. Icarus 207, 972–977 doi:910.1016/j.icarus.2009.1011.1032.

Yoshikawa, K., Nakamura, T., Igarashi, Y., 1995. Growth and collapse history of Pingos, Kuganguaq, Disko Island, Greenland. Polarforschung 64 (3), 109–113.